2001 ISMRM YOUNG INVESTIGATOR RABI AWARD PAPERS

Magnetic Resonance in Medicine 46:631–637 (2001)

Physiological Noise in Oxygenation-Sensitive Magnetic Resonance Imaging

Gunnar Krüger* and Gary H. Glover

The physiological noise in the resting brain, which arises from fluctuations in metabolic-linked brain physiology and subtle brain pulsations, was investigated in six healthy volunteers using oxygenation-sensitive dual-echo spiral MRI at 3.0 T. In contrast to the system and thermal noise, the physiological noise demonstrates a signal strength dependency and, unique to the metabolic-linked noise, an echo-time dependency. Variations of the MR signal strength by changing the flip angle and echo time allowed separation of the different noise components and revealed that the physiological noise at 3.0 T (1) exceeds other noise sources and (2) is significantly greater in cortical gray matter than in white matter regions. The SNR in oxygenation-sensitive MRI is predicted to saturate at higher fields, suggesting that noise measurements of the resting brain at 3.0 T and higher may provide a sensitive probe of functional information. Magn Reson Med 46: 631–637, 2001. © 2001 Wiley-Liss, Inc.

Key words: neuroimaging; spiral scan; magnetic field strength; SNR; physiological noise

Several biophysical models (1,2) and recent investigations of the field dependency in MRI (3–8) strongly suggest improvements in the signal-to-noise ratio (SNR) and the contrast-to-noise ratio (CNR) at higher magnetic fields. In a recent work (8), however, we have shown that the physiological noise demonstrates an MR signal strength dependency and exceeds the thermal noise and scanner noise at 3.0 T. Consequently, the physiological noise counteracts the gain in SNR at higher fields. In the present study, a model for the intrinsic noise in oxygenation-sensitive MRI of the human brain is developed. In corresponding experiments the MR-signal strength was modulated by variations in the flip angle (α) and echo-time (TE) to separate individual noise contributions in the resting brain. Results were compared with the predicted noise contributions and corresponding implications on neuroimaging modalities are discussed.

THEORY

The signal and the intrinsic noise in high-field MRI have been shown to be quadratic and linear in B_0, respectively, resulting in an SNR proportional to the strength of the magnetic field (3,4). Whereas these earlier studies characterize the dominant noise by thermally generated random noise from the subject and scanner electronics and assume that coil losses are negligible (4), we expand this model by considering physiological noise as a further significant contribution to the total image noise:

$$\sigma = \sqrt{\underbrace{\sigma_T^2 + \sigma_S^2}_{\sigma_0^2} + \sigma_P^2}. \qquad [1]$$

Here, σ_T is the thermal noise from the subject and scanner electronics and σ_S describes other system noise that includes drift and imperfections in RF, gradient, and shim subsystems. σ_0, the square-law sum of σ_T and σ_S, is considered the raw noise and has been shown to be proportional to B_0 (4) but independent of the MR-signal strength. The term σ_P in Eq. [1] describes the physiological noise, which arises from fluctuations in the basal cerebral metabolism ($CMRO_2$), blood flow (CBF), and blood volume (CBV), but also from cardiac and respiratory functions that cause quasiperiodic oscillations in the vascular system (9–11), motion from subtle brain pulsatility (12), and magnetic field modulations. In contrast to the raw noise, the herein discussed physiological noise is signal-dependent. In a more detailed consideration, we further distinguish between two different physiological noise terms, σ_B and σ_{NB}. The first contribution describes fluctuations in the transverse relaxation rate R_2^* that gives rise to small changes in the T_2^*-weighted signal, ΔS. These fluctuations, which are closely linked to brain physiology, are caused by the same mechanism that results in activation-induced signal changes in BOLD imaging and can be described by $\sigma_B = c_1 \cdot \Delta S$, where c_1 is a constant. Because of that analogy and with $dS/dR_2^* = -\mathrm{TE} \cdot S_0 \cdot \exp(-\mathrm{TE} \cdot R_2^*)$, σ_B can be expressed as:

$$\sigma_B = c_1 \cdot S \cdot \Delta R_2^* \cdot \mathrm{TE}, \qquad [2]$$

where ΔR_2^* represents the physiological fluctuation in R_2^*. Note the TE-dependency in σ_B and that σ_B demonstrates a maximum at $1/R_2^*$. The second contribution arises from image-to-image signal fluctuations due to cardiac and respiratory functions and scanner imperfections that demonstrate no TE-dependency. We can express the second contribution as $\sigma_{NB} = c_2 \cdot S$, where c_2 is a constant. Thus, the overall physiological noise

$$\sigma_P = \sqrt{\sigma_B^2 + \sigma_{NB}^2} \qquad [3]$$

is signal-dependent, as both σ_B and σ_{NB} are proportional to the signal. Because σ_P increases at the same rate as the

Lucas MRS Center, Department of Radiology, Stanford University, Palo Alto, California.

Grant sponsor: Deutsche Forschungsgemeinschaft; Grant number: Kr 1896/1-2; Grant sponsor: the NIH NCRR; Grant number: RR09784.

*Correspondence to: G. Krüger, Siemens AG, Department of MREA, Karl-Schall-Str. 6, Erlangen, 91052 Germany.
E-mail: gunnar.krueger@med.siemens.de.

Received 22 November 2000; revised 3 July 2001; accepted 3 July 2001.

2001 ISMRM Young Investigator I.I. Rabi Award Winner.

signal S, the achievable SNR at high signal strength and high magnetic fields reaches an asymptotic limit. From Eq. [1], the SNR = S/σ can be expressed as (see also Ref. [3])

$$\mathrm{SNR} = \frac{\mathrm{SNR}_0}{\sqrt{1 + \underbrace{(c_1^2 \cdot \Delta R_2^{*2} \cdot \mathrm{TE}^2 + c_2^2)}_{\lambda^2} \cdot \mathrm{SNR}_0^2}}, \qquad [4]$$

with $\mathrm{SNR}_0 = S/\sigma_0$ and $\sigma_P = \lambda \cdot S$. In this model, λ demonstrates a physical measure of the SNR-degradation by signal-dependent fluctuations, such that if $\lambda = 0$ the SNR reverts to the thermal signal-to-noise ratio, SNR_0. λ, σ_0, and σ_P are experimentally accessible by dynamic changes of the MR signal strength. Modulations of the signal, however, can be performed by changing the sequence parameter flip angle (as in this work), the echo time, or e.g., the voxel size. According to Eq. [4], changing TE can be used to distinguish the physiological noise contributions σ_B and σ_{NB}.

Fluctuations from system imperfections, e.g., in the RF and gradient subsystems, may exhibit an extremely complex behavior and may contribute to both the raw noise σ_0 and the signal-dependent physiological noise term σ_P. However, on a well-adjusted system the expected contribution from these sources to the total image noise is relatively small. Furthermore, a recent investigation (13) of image-to-image fluctuations from the disturbance of steady-state free precession (SSFP) has demonstrated that such noise components may evolve in imaging procedures for which TR $< T_2$. Because we use a TR = 3.0 sec in the current investigation, this noise source is irrelevant.

METHODS

Imaging and Scaling of Sequence Parameters

All experiments were conducted at 3.0 T (GE LX, rev. 8.25, General Electric Medical Systems, Milwaukee, WI, USA) using a custom-built transmit-receive imaging headcoil (14). Oxygenation-sensitive MRI acquisition was based on a gradient echo version of a single shot spiral sequence (15). To improve efficiency we used a dual-echo sequence. Acquisitions of both the first and the second echo started at the k-space origin and spiraled out to the maximum radius desired. A spectral-spatial RF-pulse was used to excite only water spins in the spatial slice of interest (16). After prescription of four contiguous, oblique slices (4 mm thickness, 0.5 mm gap) through the calcarine fissure the magnetic field homogeneity in the respective volume-of-interest (VOI) was improved by an automatic second-order shim correction (17), typically resulting in root mean square (RMS) fluctuations smaller than 16 Hz in the depicted VOI. For this study, we used a matrix size of 64 × 64 over a field-of-view (FoV) of 220 × 220 mm^2. This corresponds to a single-shot spiral readout window of 19.1 ms. A minimized sensitivity to inflow effects was accomplished by means of a long repetition time (TR = 3.0 sec) in all experiments. For retrospective correction of physiological motion effects, respiration and cardiac functions were monitored during the experiments using a photo-plethysmograph and a pneumatic belt, respectively (18). This image-based pixel-wise correction scheme has been shown to provide substantial reduction of the noise energy from cardiac and respiratory functions even when the noise is temporally aliased by undersampling, as in the present study (TR = 3.0 sec). Image reconstruction was performed off-line using a gridding algorithm (19). A retrospective slice-by-slice first-order shim correction was performed using a B_0-field map calculated from the first two frames with different echo-times (ΔTE = 2 ms) (20). Conventional T_1-weighted gradient echo images (TR/TE/flip = 70/5/60°) were obtained for anatomic reference and used to manually segment gray and white matter in the brain sections.

Noise Experiments

A total of six healthy subjects (age 24–34 years, 28 ± 4 years) participated in the noise imaging procedure at the 3.0 T scanner. The human protocol was approved by the Institutional Review Board of the Stanford University School of Medicine. Informed consent was obtained prior to the examinations. The subjects were instructed to close their eyes and relax in the magnet. In each session, five 7.5-min protocols with the dual-echo sequence were performed resulting in a total of 1200 frames (150 frames per slice and echo) from each trial. In order to separate the signal-dependent physiological noise σ_P from the intrinsic raw noise σ_0, we modulated the MR signal strength dynamically by alternating the flip angles between 19°, 42°, and 90° in an interleaved fashion. These particular flip angles were picked to obtain $\frac{1}{3}$, $\frac{2}{3}$, and the maximum signal. To investigate simultaneously the echo-time dependency of the physiological noise, TE combinations of 9.0 and 30.0 ms, 30.0 and 52.0 ms, 52.0 and 74.0 ms, 74.0 and 96.0 ms, as well as 9.0 and 96.0 ms were performed. Thus, each protocol with a total of 1200 frames comprised the acquisition of 50 frames per slice, echo, and flip angle.

Signal-to-Noise and Physiological Noise

The SNR and noise σ of T_2^*-weighted images were determined by calculating pixel-wise the mean signal intensity and standard deviation in the time series of 50 respective frames. The raw noise σ_0 (signal-independent noise) was determined by extrapolating from the total noise at three different flip angles to the noise at a flip angle of $\alpha = 0°$. The slope of the interpolated graph determines λ in Eq. [4]. The noise contributions σ_B and σ_{NB} in Eq. [3] were determined from the calculated λ's at five different echo times, i.e., intrinsic T_2^* values were calculated pixelwise by means of a least-squares fit of Eq. [2] to the experimental values. The SNR as well as the different noise contributions σ, σ_0, σ_B, and σ_{NB} were determined in manually drawn gray and white matter regions-of-interest (ROIs).

Phantom Noise

Identical experiments were also performed on a 17 cm diameter spherical water phantom doped with nickel-chloride in order to further characterize and validate the different noise contributions. We expected that σ_P is negligible in the phantom.

Table 1
Gray Matter Region

Subject	SNR	S_0	σ	σ_0	σ_B	σ_{NB}	λ [10^{-2}]	T_2^* [ms]
1	101.4	3261	0.54	0.21	0.42	0.27	0.9	51.8
2	57.9	4429	0.86	0.19	0.66	0.51	1.7	43.3
3	67.4	3577	0.74	0.24	0.69	0.16	1.4	48.4
4	96.4	2802	0.53	0.22	0.37	0.31	1.0	48.3
5	98.1	4395	0.55	0.17	0.52	0.0	1.0	45.0
6	82.9	2768	0.54	0.21	0.50	0.0	1.1	41.0
Mean	84 ± 18	3538 ± 740	0.63 ± .14	0.21 ± .02	0.53 ± .13	0.21 ± .20	1.2 ± 0.3	46.3 ± 3.9
Phantom	338	1137	0.19	0.14	0.08	0.08	0.2	72.8

The SNR, the signal S_0, the intrinsic noise σ, the raw noise σ_0, the physiological noise contributions σ_B and σ_{NB}, the λ-constant, and T_2^*-values in gray matter regions from all six subjects after the retrospective correction of physiological motion effects. The last row in Table 1 shows the respective values as determined in phantom experiments. S_0 demonstrates the extrapolated signal strengths at TE = 0 ms. The SNR, noise values, and λ represent the respective values at TE = 30 ms. Note that σ reflects the standard deviation in the time series and σ_0, σ_B, and σ_{NB} are determined using the model in Eqs. [1]–[4], i.e., SNR and the signal-dependent noise values σ_B and σ_{NB} reflect results with $\alpha = 90°$. For intersubject comparison noise values were normalized by the signal intensity S_0 and expressed as percentage of S_0.

RESULTS

Signal-to-Noise and Image Noise

The SNR, the signal intensity S at TE = 0 ms, the intrinsic noise σ, the raw noise σ_0, the physiological noise contributions σ_B and σ_{NB}, T_2^*-values, and λ's from the six subjects are listed in Tables 1 and 2. Table 1 represents the findings in cortical gray matter and from the phantom. Table 2 shows the corresponding results in white matter regions. All results were determined after retrospective correction of physiological motion effects and with respect to the model described above in Eqs. [1]–[4]. The noise values are normalized by the extrapolated signal intensity S_0 at TE = 0 ms and demonstrate the properties at a commonly used TE of 30.0 ms in fMRI at 3.0 T. Interestingly, the retrospective correction for physiological motion reduces the total image noise σ on average by 9 ± 2%, evenly distributed in the raw noise σ_0 (7 ± 1%) and the physiological noise contribution σ_B (10 ± 3%), and results in an increased SNR. Although σ_{NB} is also reduced in most cases, one subject showed an increase of the respective noise in gray matter regions by 2× after correction. However, in that case σ_{NB} is rather small and accounts for less than 5% of the total noise (see subject 3 in Table 1).

A spatial analysis of the noise contributions after the retrospective correction demonstrates that the raw noise σ_0 is almost identical in gray and white matter. In contrast to σ_0, the total image noise σ is found to be 1.7× greater in gray matter than in white matter regions and accounts for the observation of a significantly ($P \leq 0.01$) smaller average SNR in gray matter (SNR = 84 ± 18) than in white matter regions (SNR = 143 ± 30). Similarly, the physiological noise contribution σ_B is on average 2.1× higher in gray matter than in white matter regions and in gray matter consistently stronger than σ_0. The physiological noise contribution σ_{NB} is about 1.9× greater in gray matter regions than in respective white matter, but in magnitude a factor >2 smaller than σ_B.

Figure 1a demonstrates the physiological noise contribution σ_B in cortical gray matter regions as a function of TE averaged over all subjects. The solid line represents the best fit of Eq. [2] to the average σ_B (n = 6). The results are normalized with respect to the maximum σ_B as determined by the fit. Figure 1b shows the σ_B's from all six subjects and the best fit to the respective values. In order to emphasize the strong influence of the physiological noise to the total image noise, the individual values are normal-

Table 2
White Matter Region

Subject	SNR	S_0	σ	σ_0	σ_B	σ_{NB}	λ [10^{-2}]	T_2^* [ms]
1	165.0	3152	0.31	0.21	0.18	0.14	0.5	51.6
2	104.5	4482	0.48	0.19	0.33	0.28	0.9	44.0
3	107.4	3251	0.48	0.26	0.40	0.00	0.8	49.4
4	160.2	2604	0.33	0.23	0.17	0.15	0.5	50.9
5	174.0	4154	0.32	0.20	0.24	0.00	0.5	51.4
6	150.5	2466	0.32	0.24	0.18	0.11	0.5	46.5
Mean	143 ± 30	3351 ± 814	0.37 ± .08	0.22 ± .03	0.25 ± .10	0.11 ± .11	0.6 ± 0.2	49.0 ± 3.1

The SNR, the signal S_0, the intrinsic noise σ, the raw noise σ_0, the physiological noise contributions σ_B and σ_{NB}, the λ-constant, and T_2^*-values in white matter regions from all six subjects after the retrospective correction of physiological motion effects. The SNR, noise values, and λ represent the respective values at TE = 30 ms. For intersubject comparison noise values were normalized by the signal intensity S_0 and expressed as percentage of S_0.

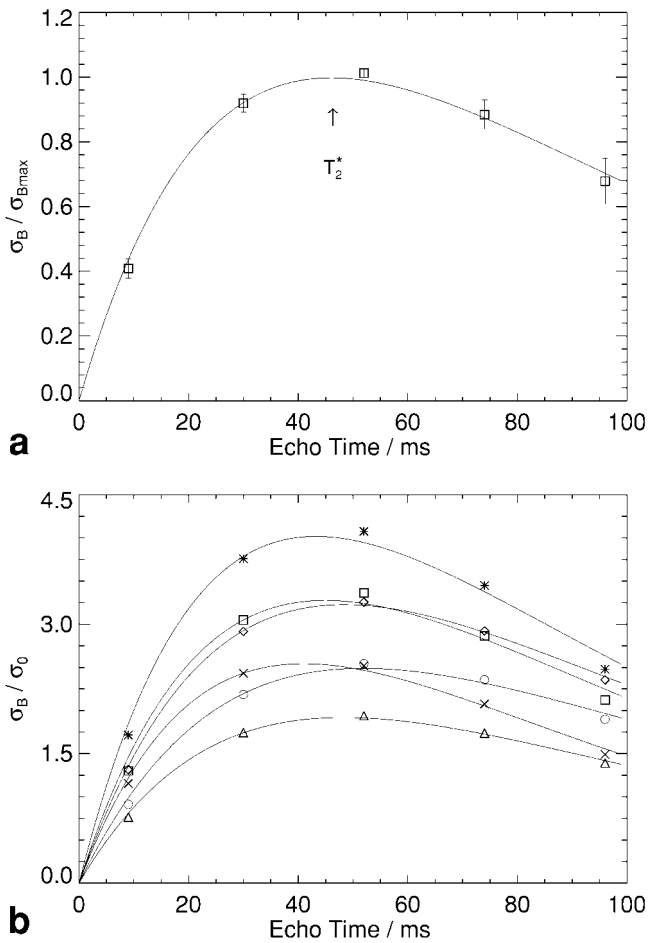

FIG. 1. The mean (n = 6) physiological noise contribution σ_B as a function of TE in cortical gray matter regions (**a**). For the intersubject comparison, σ_B's were individually normalized by the interpolated noise at TE = T_2^* prior to averaging. The symbols represent the mean noise and the solid line shows the best fit of Eq. [2]. Errors bars (±SD) represent the variability across subjects. **b:** σ_B as a function of TE from all six subjects. Here, the individual graphs were normalized by the respective raw noise σ_0.

ized by the corresponding raw noise σ_0. Note that results from an individual subject represent an average value over four slices and two trials per echo time. The corresponding results in white matter regions are shown in Fig. 2a,b. σ_B clearly demonstrates in both white and gray matter regions the expected echo-time dependency of Eq. [2] with a maximum at the intrinsic T_2^*-relaxation time. Thereby determined transverse relaxation times revealed $T_2^* = 46.3 \pm 3.9$ ms in gray matter and $T_2^* = 49.0 \pm 3.1$ ms in white matter regions, as denoted in the plots and in good agreement with recently published data (8,21).

Noise measurements on the phantom also exhibited signal-dependent contributions. However, the corresponding λ coefficient at TE = 30 ms (Table 1) is approximately 6× and 3× smaller than measured λ's in cortical gray and white matter, respectively. The residual "physiological" noise contribution in the phantom may arise from vibrations of the water in the fluid-filled phantom on the patient table or from system imperfections. Thus, σ_P measured on the phantom reflects the individual noise properties of the particular sequence and scanner. Due to the square-law summation of all noise contributions to the total image noise (see Eq. [3]), σ_P in the phantom is of only small influence on σ, and cannot explain the dominance of the physiological noise in the human subjects at 3.0 T.

Spatial Distribution of Noise Components

The spatial distributions of several noise sources in an exemplary slice from one subject and in the phantom are shown in Fig. 3. Figure 3a demonstrates a high resolution MRI of the section. Figure 3b–d represents the raw noise σ_0, the physiological noise contribution σ_B, as well as the noise contribution σ_{NB} in the same slice at TE = 30 ms. Both the σ_0-map (Fig. 3b) and the σ_{NB}-map (Fig. 3d) demonstrate a rather uniform distribution of noise. However, the σ_B-map (Fig. 3c) clearly exhibits spatial differences in the noise, showing larger noise in gray matter regions. Higher noise values at the frontal brain area in the σ_{NB}-map (Fig. 3d) presumably reflect slight subject motion. The phantom raw noise in Fig. 3e exhibits a slight spatial gradient that may reflect a B_1 heterogeneity from the RF-coil sensitivity profile. The focal regions in the respective

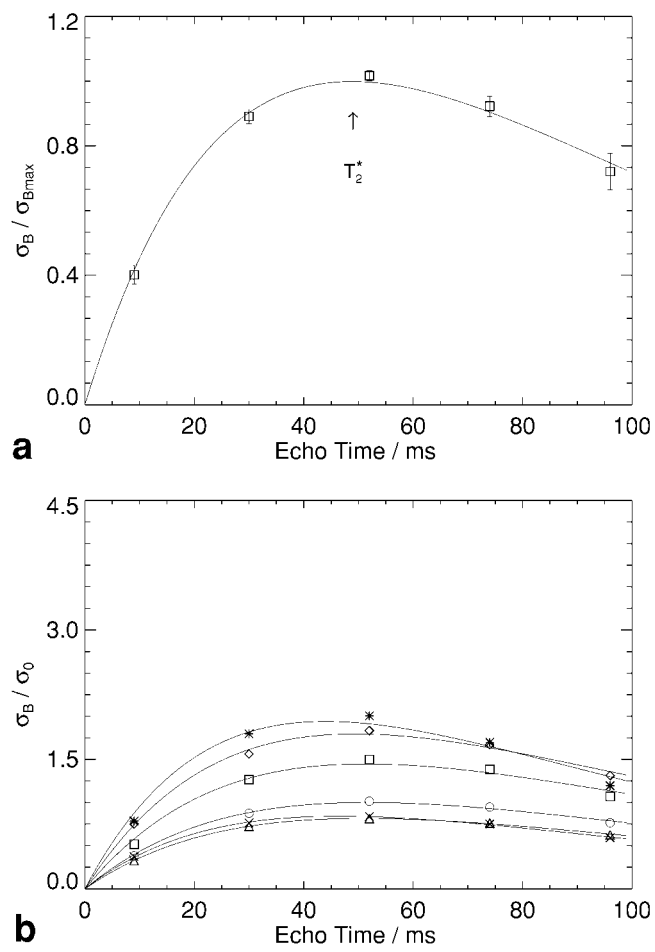

FIG. 2. The corresponding physiological noise contribution σ_B in white matter.

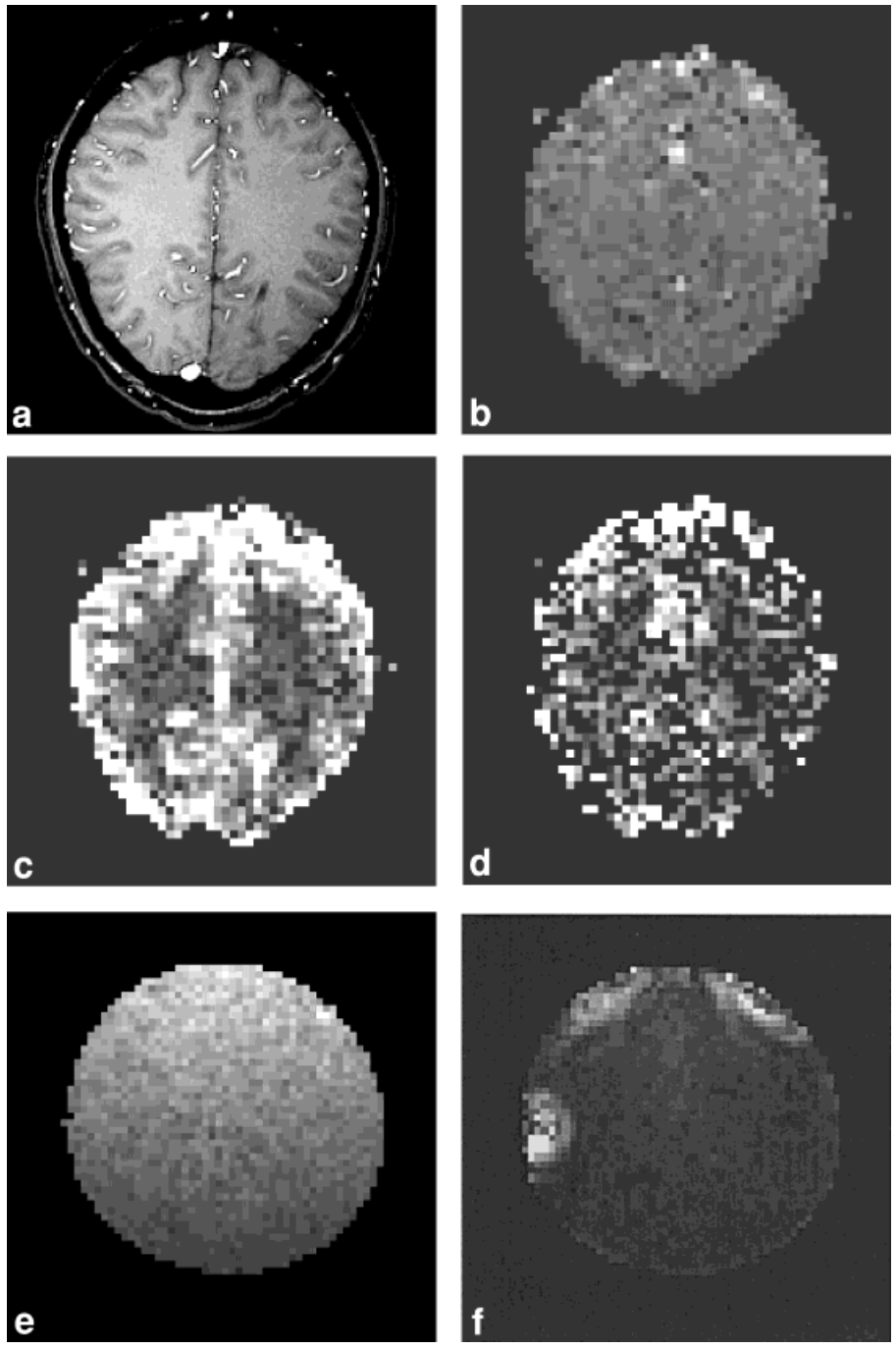

FIG. 3. Anatomy (**a**) and spatial distribution of raw noise σ_0 (**b**), physiological noise contributions σ_B (**c**), and σ_{NB} (**d**) in a typical image section from one subject. Note that gray scale contrast is identical in **b–d.** Corresponding maps of σ_0 and σ_B from the phantom are shown in **e** and **f,** respectively.

σ_B-map (Fig. 3f) are presumably due to vibrations of water in the phantom near regions of altered susceptibility from a label attached to the phantom and a plug that fills a hole used for filling the phantom with water. However, in this work we propose only a simple model of the noise in GRE imaging, and therefore such effects, as well as obvious vascularity (e.g., in the center of the anatomical slice in Fig. 3a), violates this simple model.

DISCUSSION

The proposed model in Eqs. [1]–[4] for SNR and noise properties in gradient-echo (GRE) MRI suggests that the physiological noise increases with the signal strength and limits the maximum attainable SNR at a ratio of $1/\lambda$. The mean λ values across six subjects, e.g., at TE = 30 ms, of $\lambda_{gm} = 0.012 \pm 0.003$ and $\lambda_{wm} = 0.006 \pm 0.002$ predict that the maximum attainable SNR in gray matter regions amounts to SNR = 83 in cortical gray matter and to SNR = 167 in white matter regions for the acquisition parameters and hardware used here. The respective SNR of 84 and 143 obtained in the present study are close to these predicted asymptotic SNR-values of $\sim 1/\lambda$ and imply that further improvements in coil and magnetic field strength would yield only moderate additional gains in SNR. It can be argued that TR = 3.0 sec is not sufficient to suppress the

development of steady-state magnetization in the post-90°-pulse images in voxels that are contaminated by CSF. However, in a recent study (8) we investigated the physiological noise term σ_P with repetition times of TR = 3.0 ms and TR = 5.4 sec. The finding of very similar λ's at both TRs demonstrates that the calculated noise terms can be considered to be nearly uninfluenced by saturation effects. This results because the CSF signal was greatly suppressed by the use of RF spoiling, and contamination from CSF was minimized.

The retrospective correction scheme applied here (18), corrects effectively for respiration- and cardiac-induced periodic fluctuations in R_2^* and reduces the corresponding noise energy to the average noise level. More explicitly, we observed a 7% decrease in σ_0 and a 10% decrease in σ_B. However, fluctuations in brain metabolism and neuronal activity and the related physiological changes in CBF, CBV, and $CMRO_2$ cause signal changes due to a true BOLD-effect and are unaffected by those correction schemes. Considering the favorable motion insensitivity of spiral imaging (12) that minimizes the motion-related contributions in σ_P in combination with the concomitant correction method (18), we believe that the remaining σ_B as presented here is primarily characterized by fluctuations directly linked to brain metabolism and neuronal activity and potentially reflects resting-state activity or a certain level of neuronal brain activity. Moreover, changes in the fluctuations of brain metabolism, CBF, and CBV may evoke temporal and/or spatial correlations of the physiological noise. Thus, investigation of the noise rather than the signal only may have great potential in functional neuroimaging.

A regional analysis of the physiological noise contribution σ_B in the "resting" brain clearly exhibited stronger signal fluctuations in the cortical gray matter than in white matter regions, as shown in earlier work (8,9). Moreover, at TE = 30 ms σ_P is 1.2× (white matter) and 2.7× (gray matter) greater than the respective raw noise σ_0. Thus, the physiological noise, which is dominated by σ_B, is not only responsible for the observation of the lower SNR in gray matter regions but also represents the dominant noise source in the image noise in long echo-time fMRI experiments at 3.0 T and therefore determines the attainable SNR. Because all physiological noise contributions are signal-dependent, they become larger with stronger signals as obtained at higher fields and with improved surface coils. σ_0, which is dominated by thermal noise from the subject, demonstrates very similar magnitude of 0.21 ± 0.02 and 0.22 ± 0.03 in gray and white matter regions. This is in line with the expectation that σ_0 should be independent of signal strength and supposedly independent across different brain tissues (4). The finding of a rather uniform distribution of σ_0 across brain tissue, but significant regional differences in σ_B, is visually supported in Fig. 3, as the σ_B-map in Fig. 3c clearly exhibits lower noise in white matter regions and higher noise values in the respective cortical gray matter areas (compare Fig. 3a).

It is worthwhile to consider that inhomogeneities in the B_0-field and in transmit-receive coil systems may lead to misinterpretations of the spatial distribution of the noise. Coil inhomogeneities cause a spatial dependency of the B_1-field. Subsequently, this leads to spatial heterogeneities of the MR signal intensity and of the signal-dependent physiological noise. These phenomena could explain the remaining heterogeneity in Fig. 3b and e and the slightly more pronounced physiological noise in the frontal edge of the brain in Fig. 3c and d. As suggested by one referee, the additional use of a spin-echo technique could be used to further investigate the composition of the two noise sources σ_B and σ_{NB}, as the TE-dependent physiological noise contribution theoretically disappears in spin-echo images.

Recently published preliminary results from a comparison of SNR and noise properties at 1.5 T and 3.0 T using conventional EPI (22) have also reported that physiological noise appears to be more dominant at higher fields. In that study, the signal strength was modulated by a variation of TE. The present results, however, clearly suggest that the physiological noise consists of at least two different contributions, one of them with a TE-dependency. Therefore, it is necessary to modulate the signal without changing TE (e.g., using the flip angle as in this work) in addition to obtaining measurements with different TE's to separate the two noise components.

CONCLUSIONS

The present results demonstrate that the image noise in oxygenation-sensitive neuroimaging at 3.0 T is decisively dominated by the physiological noise. This is due to the fact that σ_P, σ_B, and σ_{NB} are signal-dependent and increase with improved RF-coils and field strength. σ_B, which demonstrates the primary contributor to σ_P, is found to be 2.1× higher in cortical gray matter than in white matter regions and therefore limits the maximum attainable SNR and CNR in MRI at higher fields. However, this noise source also may reveal important information on brain physiology, as it represents fluctuations in CBF, CBV, and oxidative metabolism. Strategies such as investigations of functional connectivities and event-related fMRI, which analyze spatial and temporal correlations of signal fluctuation time courses (noise), are predicted to benefit from the increased influence of σ_P at higher fields.

ACKNOWLEDGMENTS

The authors thank A.M. Sawyer-Glover for assistance and T.J. Brosnan for technical support.

REFERENCES

1. Fisel CR, Ackerman JL, Buxton RB, Garrido L, Belliveau JW, Rosen BR, Brady TJ. MR contrast due to microscopically heterogeneous magnetic susceptibility: numerical simulations and applications to cerebral physiology. Magn Reson Med 1991;17:336–347.
2. Ogawa S, Menon RS, Tank DW, Kim SG, Merkle H, Ellermann JM, Ugurbil K. Functional brain mapping by blood oxygenation level-dependent contrast magnetic resonance imaging. A comparison of signal characteristics with a biophysical model. Biophys J 1993:64:803–812.
3. Hoult DI, Lauterbur PC. The sensitivity of the zeugmatographic experiment involving human samples. J Magn Reson 1979;34:425–433.
4. Edelstein WA, Glover GH, Hardy CJ, Redington RW. The intrinsic signal-to-noise ratio in NMR imaging. Magn Reson Med 1986;3:604–618.

5. Turner R, Jezzard P, Wen H, Kwong KK, Le Bihan D, Zeffiro T, Balaban RS. Functional mapping of the human visual cortex at 4 and 1.5 Tesla using deoxygenation contrast EPI. Magn Reson Med 1993;29:277–279.
6. Gati JS, Menon RS, Ugurbil K, Rutt BK. Experimental determination of the BOLD field strength dependence in vessels and tissue. Magn Reson Med 1997;38:296–302.
7. Yang Y, Wen H, Mattay VS, Balaban RS, Frank JA, Duyn JH. Comparison of 3D BOLD functional MRI with spiral acquisition at 1.5 T and 4.0 T. NeuroImage 1999;9:446–451.
8. Krüger G, Kastrup A, Glover GH. Neuroimaging at 1.5 T and 3.0 T: comparison of oxygenation-sensitive magnetic resonance imaging. Magn Reson Med 2001;45:595–604.
9. Weisskoff RM, Baker J, Belliveau J, Davis TL, Kwong KK, Cohen MS, Rosen BR. Power spectrum analysis of functionally-weighted MR data: What's in the noise? Proc ISMRM 1993;1:7.
10. Bandettini PA, Wong EC, Jesmanowicz A, Prost R, Cox RW, Hinks RS, Hyde JS. MRI of human brain activation at 0.5 T, 1.5 T, and 3.0 T: comparison of δr_2^* and functional contrast to noise ratio. Proc ISMRM 1994;1:434.
11. Biswal B, Yetkin FZ, Haughton VM, Hyde JS. Functional connectivity in the motor cortex of resting human brain using echo-planar MRI. Magn Reson Med 1995;34:537–541.
12. Glover GH, Lee AT. Motion artifacts in fMRI: comparison of 2DFT with PR and spiral scan methods. Magn Reson Med 1995;33:624–635.
13. Zhao X, Bodurka J, Jesmanowicz A, Li S-J. B0-fluctuation-induced temporal variation in EPI image series due to the disturbance of the steady-state free precession. Magn Reson Med 2000;44:758–765.
14. Fitzsimmons JR, Scott JD, Peterson DM, Wolverton BL, Webster CS, Lang PJ. Integrated RF coil with stabilization for fMRI human cortex. Magn Reson Med 1997;38:15–18.
15. Glover GH. Simple analytic spiral k-space algorithm. Magn Reson Med 1999;42:412–415.
16. Meyer CH, Pauly JM, Macovski A, Nishimura DG. Simultaneous spatial and spectral selective excitation. Magn Reson Med 1990;15:287–304.
17. Kim DH, Adalsteinsson E, Glover G, Spielman DM. SVD regularization algorithm for improved high-order shimming. Proc ISMRM 2000;3:1685.
18. Glover GH, Lie TQ, Rees D. Image-based method for retrospective correction of physiological motion effects in fMRI: RETROICOR. Magn Reson Med 2000;44:162–167.
19. Meyer CH, Hu BS, Nishimura DG, Macovski A. Fast spiral coronary artery imaging. Magn Reson Med 1992;28:202–213.
20. Glover GH, Lai S. Self-navigated spiral fMRI: interleaved versus single-shot. Magn Reson Med 1998;39:361–368.
21. Wansapura JP, Holland SK, Dunn RS, Ball WAS. NMR relaxation times in the human brain at 3.0 T. J Magn Reson Imag 1999;9:531–538.
22. Petridou N, Bandettini PA. Comparison of the TE and field strength dependence of single shot image S/N and time series standard deviation in humans and phantoms. Human Brain Mapping, 6th Annual Meeting, San Antonio, TX, USA, June 12–16. NeuroImage 2000;11(5):677.